A Novel Incipient Fault Detection Technique for Roller Bearing Using Deep Independent Component Analysis and Variational Modal Decomposition

Vishal G. Salunkhe
Department of Mechanical Engineering,
Fr. C. Rodrigues Institute of Technology,
Vashi, Navi Mumbai, Maharashtra 400703, India
e-mail: vishalsalunkhe84@gmail.com

R. G. Desavale[1]
Design Engineering Section,
Department of Mechanical Engineering,
Rajarambapu Institute of Technology,
Rajaramnagar, Sakharale, Sangli,
Shivaji University,
Kolhapur, Maharashtra 415414, India
e-mail: ramchandra.desavale@ritindia.edu

S. M. Khot
Department of Mechanical Engineering,
Fr. C. Rodrigues Institute of Technology,
Vashi, Navi Mumbai, Maharashtra 400703, India
e-mail: smkhot66@yahoo.co.in

Nitesh P. Yelve
Department of Mechanical Engineering,
Indian Institute of Technology Bombay,
Powai, Mumbai, Maharashtra 400076, India
e-mail: nitesh.yelve@iitb.ac.in

Roller bearing failure can result in downtime or the entire outage of rotating machinery. As a result, a timely incipient bearing defect must be diagnosed to ensure optimal process operation. Modern condition monitoring necessitates the use of deep independent component analysis (DICA) to diagnose incipient bearing failure. This paper presents a deep independent component analysis method based on variational modal decomposition (VMD-ICA) to diagnose incipient bearing defect. On a newly established test setup for rotor bearings, fast Fourier techniques are used to extract the vibration responses of bearings that have been artificially damaged using electro-chemical machining. VMD techniques diminish the noise of the measurement data, to decompose data processed into multiple sub-datasets for extracting incipient defect characteristics. The simplicity of the VMD-ICA model enriched the precision of diagnosis correlated to the experimental results with weak fault characteristic signal and noise interference. Moreover, deep VMD-ICA has additionally demonstrated strong performance in comparison to experimental results and is useful for monitoring the condition of industrial machinery. [DOI: 10.1115/1.4056899]

Keywords: rolling bearing, incipient defect, vibration analysis, deep independent component analysis, rolling element bearings

1 Introduction

Rolling element bearings, like a ball, cylindrical, or conical rolling bearing, are majorly used in power generation industries, process industries, machine tools, and automobiles. The rolling bearing is repeatedly invoked as anti-friction bearing. When preferred and appropriately tested, they can operate effectively over a lengthy duration of time. A rolling element bearing's average lifespan is known because of fatigue behavior. Ball bearings implicate a point association betwixt the races and the balls, which produces high stress at the contact. Failure of bearings causes deficient of the machines and abandon, which impacts the final product's price and quality. Anti-friction bearings are believed to be responsible for 30% of machinery failures. As a result, bearing condition monitoring in rotating machinery is extremely crucial. A new regulating instrument for the shift from reactive to proactive is condition-based monitoring in industries. Premature failures can be identified and analyzed with the help of conditional monitoring, which reduces downtime and costs.

Different fault diagnosis techniques are developed and utilized efficiently to forecast imminent machine failures at their current stage. Some include vibration analysis, oil debris analysis, nondestructive testing, thermal, noise, motor current analysis, component error, oil flowrate, oil viscosity, and statistical features. It is among the most common methods for analyzing vibration. Using experimentation or model-based techniques, one can forecast the health status of bearings in rotating machinery's by analyzing vibration signatures. The model-based technique can convert complex engineering problems into simplified mathematical models. The model-based theoretical approach builds the circumstances for the effectiveness of experiments and evaluation of mathematical models with experimental results. Therefore, the model-based vibration conditioning monitoring techniques have been to pick up in-depth study throughout the earlier decades. Using signal processing techniques makes it feasible to attain significant characteristic frequency from the vibration signals. The present work uses the innovative technique of model-based study to determine the effect of speed, load, surface defects size, and other physical parameters on bearing failure.

Stefatos and Hamza [1] developed Tennessee Eastman challenge technique by independent component analysis (ICA)-based methodology to identify the primary source of the fault. Fan and Wang [2] proposed kernel-dynamic independent component analysis for fault identification. Plotting of non-linear contribution with Tennessee Eastman process showed greater effectiveness. Mao et al. [3] developed deep transfer learning with a pre-trained VGG 16 model for fault identification in auxiliary bearing. Deep features with fine-tuning technique are used for training model with support vector machine.

Cai et al. [4] developed noisy independent component analysis for condition monitoring. Fourth order cumulant matrix with joint diagonalization is estimated by noisy intercluster separation algorithm. Three variable system with stirred tank reactor system detects fault by recursive independent component kurtosis. Cai and Tian [5] investigated robust independent component analysis (Robust ICA) algorithm for extracting non-Gaussian features for robust whitening and determination. Cai et al. [6] developed a model for milling chatter with energy entropy and variational mode decomposition (VMD). Number of modes with quadratic penalty is an input function to VMD for kurtosis selection with total energy absorbed by frequency band. Simulation and

[1]Corresponding author.

Contributed by the Tribology Division of ASME for publication in the Journal of Tribology. Manuscript received October 7, 2022; final manuscript received January 28, 2023; published online April 3, 2023. Assoc. Editor: Nick Weinzapfel.

experimental signals were used for extraction of chatter feather for model effectiveness. Wang et al. [7] demonstrated constrained independent component analysis (cICA) for recovering intended defective signal. Simulation and experimentation findings show higher efficiency of cICA for machine diagnosis. Yu et al. [8] combined envelope extraction and independent component analysis for impulsive component to identify faults in bearing. Envelopes are separated according to independent vibration sources using ICA. Simulation and experimental findings are validated and show a good correlation. Iseli et al. [9] analyzed the dynamic characteristics of spiral grooved gas journal bearing at diverse compressibility quantities, grooves, and eccentricities by narrow-groove theory and finite element analysis (FEA). Quasi-steady-state with pressure characteristics is formulated with a time-periodic technique. Benwei and Yun [10] investigated a supervised locally linear embedding projection (SLLE) technique for fault identification in machinery. Fault classification performance significantly improved using the SLLE approach.

McFadden and Smith [11,12] developed a numerical model for rolling element bearing operating in radially loading conditions for predicting the inner defect. Defects are modeled as spectrum of instinct caused by roller passage frequency for the inner race. Their model also can be used to detect multiple defects in bearings. Patil et al. [13] reported on vibration responses generated in ball-bearing due to localized defects and found that vibration amplitude is on the higher side due to an increment in the size of the speed, load, and defect. Dick et al. [14] elaborated a model of varying stiffness of double row rolling element bearing under radial load and quasi-static load distribution. When a defect exists, bearing stiffness changes rapidly due to parametric excitation of bearing assembly. High contact impulsive forces are observed, which wobble all around quasi-static force on the rollers, due to swift change in stiffness.

Igarashi and Kato [15] developed time delay functions for defects on the outside race and inside the race and analyzed defects size on vibration responses. Sopanen and Mikola [16,17] formulated an analytical model for localized and distributed flaws in a spherical roller bearing, and lubrication effects and non-linear Hertz contact deformation have been analyzed. Tandon and Choudhary [18] developed a numerical model for prognoses of vibrational frequency due to the localized and distributed defects. Due to defects, the gradual increment in vibration amplitudes leads to increased machine vibrations with higher frequency. Tandon and Choudhary [19] illustrated a numerical model to predict the responses of bearings under radially loading conditions due to unevenly distributed defects. The model foretells discrete spectrum responses at both inner and outer ring defect frequencies. In healthy bearing, the amplitude levels are on the lower side as compared with defective bearing.

Tandon and Choudhury [20] considered vibrations of bearing with different defect sizes. The three degrees-of-freedom (DOF) system is modeled for the rotor-bearing system. The sideband peaks at defect frequencies, cage frequencies, and shaft frequencies, can be predicted using their model. Tomovic et al. [21] proposed a realistic novel vibrating model for a sturdy rotor-bearing structure. They analyze the consequence of inside clearance and the sum of rollers on rigid rotor vibration. Desavale et al. [22,23] applied dimensional analysis to model vibrational problems due to local flaws in the forced draft fans bearings. Taguchi technique is used to carry out a multivariable regression analysis. The authors compared experimental results with numerical models developed using dimensional analysis and found close agreement between the two. Desavale et al. [24,25] investigated the consequences of rotating speed, radial load, with various other factors on vibration responses by building a model for the rotor-bearing structure. The authors also studied rotor misalignment inaccurately fitted in the bearing using dimensional analysis. Mathematical models using non-dimensional parameters are developed to analyze the rotor-bearing structure.

Mufazzal et al. [26] developed lumped system with two DOF with multi-impact theories for simulating healthy and defective bearings. Patil et al. [27] illustrated vibrational characteristics responses for different loads, speeds, defect sizes, and locations. Kanai et al. [28] formulated a unique and simplified technique for deep-grove ball bearing (DGBB) fault detection using an artificial neural network with condition-based rotating system monitoring. Patel et al. [29] conferred a theoretical model for bearing with sole and different faults on both inner and outer races. Governing equation of coupled solution is attained by using the Runge–Kutta technique.

Liu [30] obtained an analytical model for rotor roller-bearing housing structure for resonance at the contact area due to raceways faults, deformation at housing due to the rotor and outer race, and oil film thickness. Hertzian contact theory determines time depending on increased contact area and relative motion among roller and faults. The time depended on the function of half-sine with resonance model is used to formulate displacement resonance due to fault. Niu et al. [31] illustrated a model for cylindrical roller bearing with cracks on both the races. Factors like slippage, roller diameter, and contact force are considered, and vibration responses are investigated when the roller oscillates around the races.

Rafsanjani et al. [32] examined a statistical model that could predict bearing vibration characteristics produced by a surface fault. Diverse non-linear dynamic conditions are also enormously influential in forecasting the presence of surface pitting at corresponding characteristic frequencies in bearing. Yang et al. [33] investigated an analytical model which utilizes the oscillating intensity of bearing with varying compliance vibration responses in the different speed ranges, number of balls, and rotor eccentricities. Jadhav et al. [34] demonstrated the power of dimension theory to detect distributed defects. Kumbhar et al. [35,36] presented a dynamic model with geometric, thermal, and operational parameters of structure for spherical roller bearing by using dimension theory. The identification of exact bearing failure and effectiveness of the theoretical model is accomplished with multivariable regression analysis. Salunkhe et al. [37] formulated a model by dimensional analysis using a matrix technique to forecast the vibrations associated with dependent parameters. Formulated model is solved numerically by SVM. The influences of various parameters like rotor speed, bearing faults are studied by SVM. Londhe et al. [38] investigated FEA analysis for dynamic capacity in materials for considering plastic deformations. Liu et al. [39–41] developed a model for cylindrical roller bearing of oil jet lubrication in a gearbox. Temperature differences are analyzed and compared for lubricating characteristics. The effect of edge defect length and contact stiffness accelerates higher peaks in vibration signatures. Statistical features with spalling assessment algorithms are used to identify actual fault position and its severity on operation. Yan et al. [42] illustrated enhanced adaptive VMD technique for rotor fault identification. Internal variables of VMD are determined by gray wolf optimization with weighted sparseness kurtosis for target optimization. Promising demodulation performance is attained with the Teager energy operator for time-frequency representation. Fu et al. [43] proposed a framework for fault diagnosis of roller bearing with VMD by expanding features of faulty signals. Principal component analysis (PCA) and multi-information

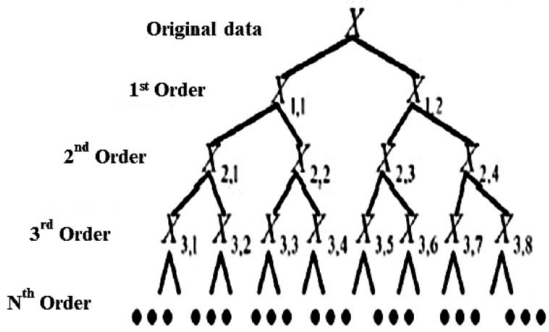

Fig. 1 Principal of deep composition

fusion with a support vector machine incorporated for classification accuracy.

However, no research published to date that presents an effective integration deep independent component analysis (DICA) approach based on variational modal decomposition (VMD-ICA), which is the novelty of the present work. This research contributes to the use of VMD-ICA modeling for the detection and classification of incipient bearing failures. This is the first study in the realm of roller-bearing diagnosis that synchronizes the robustness and accuracy of VMD-ICA.

A literature review indicates that deep VMD-ICA distinct mathematical models have been used extensively for vibration analysis of industrial machines. Simple mathematical models cannot represent a complex industrial system. Hence, many studies reported the potential of the deep ICA due to its simple and unique combination of analytical with the experimental approach for predicting the vibration characteristics. Even mathematically modeled well, they cannot expose the critical non-linear or anisotropic material characteristics encountered generally in practice. There is scope to integrate these two powerful methods for vibration analysis of rotor systems. Hence, deep VMD-ICA is used to investigate the effect of the incipient fault in a DGBB. First, VMD-ICA model formulation is presented, which stimulates the vibrational characteristics subsequently. The estimated routine performance of the developed VMD-ICA model is compared with the experiments. Experimental investigations verify the prediction of vibration characteristics using VMD-ICA for incipient fault classification. Proposed method takes into account the influence of noise on detection and fully excavates incipient fault information. Finally, the conclusion and scope for future work are revealed. The present method is suitable for monitoring rotating machines such as CNC, fibrizer, ID fan, FD fan, and centrifugal machines in sugar industries.

2 Establishment of the Theoretical Model for Contact Ball Race

2.1 Mathematical Model of Variational Modal Decomposition. Variational modal decomposition is an adaptive technique of modal variation and signal processing, which decomposes and restructures the signal to gain multiple eigen mode components (IMF). The mathematical model can be given by an equation of the form [6]

$$\left\{\delta(t)+\frac{i}{\pi t}\right\} * \mu_k(t) \tag{1}$$

The Hilbert transform is used for demodulation. By estimating the bandwidth of each modal of the demodulated signal, the variational problem with constraints is expressed as

$$\left\{\min_{(u_k)(w_k)}\left\{\sum_k^i\left[\delta[(t)]+\frac{i}{\pi t}u_k(t)\right]e^{-iw_k t}\right\}\text{s.t}\ \sum_k^i u_k = f\right\} \tag{2}$$

where, $u_k=(u_1,\ \ldots,\ u_k)$ represents all modes and $w_k=(w_1,\ \ldots,\ w_k)$ represents their center frequency. It is to be noticed that to solve the aforementioned variational constraint problem, a secondary forfeiture factor α is introduced. To ensure that the signal can be accurately decomposed under the influence of Gaussian noise and the Lagrangian multiplier λ. The following model can be built, Eq. (3) may be written as

$$L([u_k],[w_k],[\lambda]) = \alpha\sum_{k=1}^{K}\delta_t\left[(\delta_t)+\frac{i}{\pi t}\right]u_k(t)e^{-iw_k t} + f(t)\sum_{k=1}^{K}u_k(t)+\lambda(t), f(t)-\sum_{k=1}^{k}u_k(t) \tag{3}$$

The above Eq. (3) uses the alternate multiplier algorithm to alternately update the u_k^{n+1}, w_k^{n+1}, λ_k^{n+1} to solve optimal solution of the augmented Lagrangian function.

2.2 Independent Component Analysis Method. In addition to the matter of blind source separation, independent component analysis, is a novel data analysis technique proposed in the 1990s. Its appearance is to solve the problem of separating each independent component by processing the actual observation signal when multiple independent and unknown blind source signals are mixed together. According to the basic principles of ICA [1], can be expressed using Eq. (4)

$$X = AS + E \tag{4}$$

where, $X=(x_1^t,\ldots,\ x_n^t)^T \in \gamma^{l*n}$ is a matrix of process data, $S=(s_1,\ s_2,\ \ldots,\ s_n)^T \in \gamma^{m^*n}$ is the matrix representing the IC. $A=\ (a_1,\ \ldots,\ a_n)^T \in \gamma^{l^*m}$ is a mixing matrix and $E=\ \in \gamma^{l^*n}$ indicates residual matrix. Using the ICA method to find the separation matrix W to reconstruct the source signal matrix S, can be obtained as

$$S = WX \tag{5}$$

Online measurement data detection aims to analyze and interpret the measurement results to detect faults continuously. The ICA detection model mainly includes two parts: offline modeling and online detection.

2.3 Formulation of VMD-DICA Algorithm. The fault detection model based on deep VMD-ICA algorithm proposed mainly includes the following three parts. The first part: use VMD to process the collected measurement data to reduce noise interference. The second part: introduce the deep decomposition principle to extract incipient fault characteristics from the data processed by VMD. The third part: establish ICA fault detection model to complete incipient fault detection [40]. The preprocessed signal is divided into many multi-component signals using VMD and optimal variables [42].

2.3.1 Extraction of Incipient Fault Features. The principle of deep decomposition is based on principal component analysis, which decomposes the original dataset into two subspaces, where the main subspace can retain a large amount of variance information of the original dataset. Using the principle of deep decomposition is to use the feature decomposition method of PCA to decompose the dataset by λ-order, and then generate 2^λ sub-datasets. In this way, incipient fault characteristics are simple to extract. The principle of deep decomposition is shown in Fig. 1.

2.3.2 Deep Decomposition Theory. First, using the principle of deep decomposition, the first-order decomposition results of the data X_c are written as

$$X_c = X_{c11} + X_{c12} \tag{6}$$

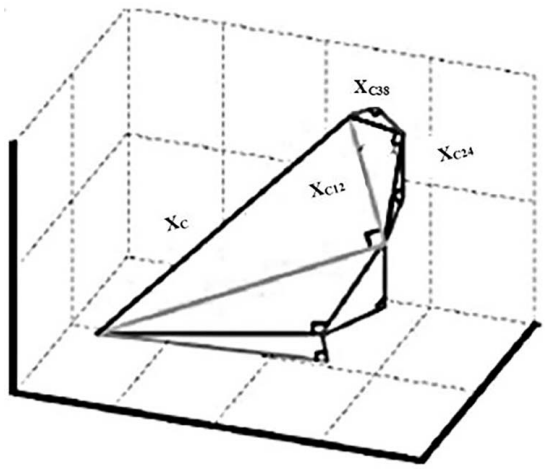

Fig. 2 Geometric decomposition of deep VMD-ICA method

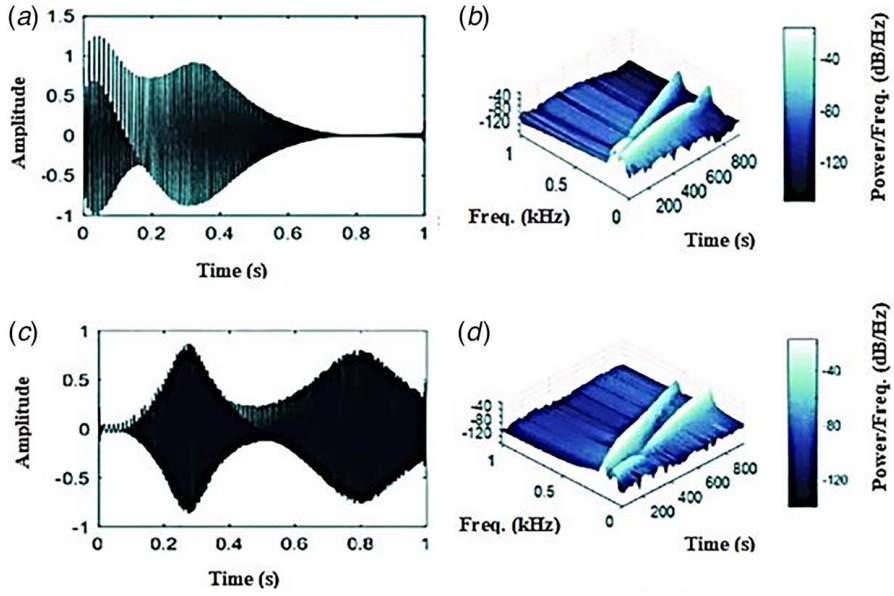

Fig. 3 Vibration amplitude of VMD decomposition

Here, X_{c11} is the principal component space of the first-order decomposition of the original data, and X_{c12} is the residual subspace of the first-order decomposition. According to the principle of deep decomposition, they can be obtained as

$$X_{c11} = P_{11}P_{11}^{T}X \tag{7}$$

$$X_{c12} = (I - P_{11}P_{11}^{T})X \tag{8}$$

where, P_{11} the eigenvector corresponding to the principal component space, and the second-order decomposition result P can be calculated

$$X_{c11} = X_{c21} + X_{c22} \tag{9}$$

$$X_{c12} = X_{c23} + X_{c24} \tag{10}$$

Later, the initial dataset can be decomposed as

$$X_c = X_{c11} + X_{c12} = X_{c21} + X_{c22} + X_{c23} + X_{c24} \tag{11}$$

$$X_{c21} = (P_{21}P_{21}^{T})X_{c11} \tag{12}$$

$$X_{c22} = (I - P_{21}P_{21}^{T})X_{c11} \tag{13}$$

$$X_{c23} = (P_{23}P_{23}^{T})X_{c12} \tag{14}$$

$$X_{c24} = (I - P_{23}P_{23}^{T})X_{c12} \tag{15}$$

Assuming, $P_{(\lambda+1)(2k-1)}$ is the main load vector related to after λ-order decomposition, $X_{c\lambda k}$ can be expressed as

$$X_{c\lambda k} = \left| \frac{P_{\lambda k}P_{\lambda k}^{T}X_{c\lambda-1(k+1)\div 2}}{(I - P_{\lambda k}P_{\lambda k}^{T})X_{c\lambda-1\,k\div 2}} \right| \tag{16}$$

As the dataset is continuously decomposed by the principle of deep decomposition, the incipient weak fault characteristics can be extracted to the greatest extent, and the expected fault detection effect can be achieved.

2.3.3 Analytical Theory. This section explains the incipient fault detection capability of deep VMD-ICA from the perspective of theoretical analysis. However, time lags and auto-correlation should not underestimate in dynamic processes. The deep decomposition is the same as the PCA feature extraction principle, and the only difference between the two is that PCA only performs first-order feature decomposition on the original dataset, while the deep decomposition uses the PCA decomposition principle to perform multi-order decomposition on the original data. In the process of decomposition, the amount of information stored is usually measured by the size of the covariance. Assume that, the

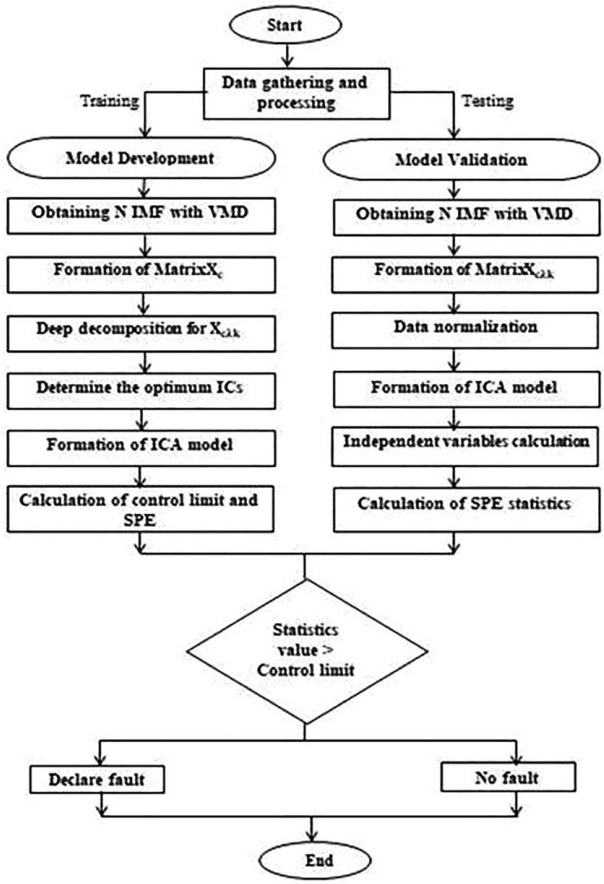

Fig. 4 Deep VMD-ICA algorithm

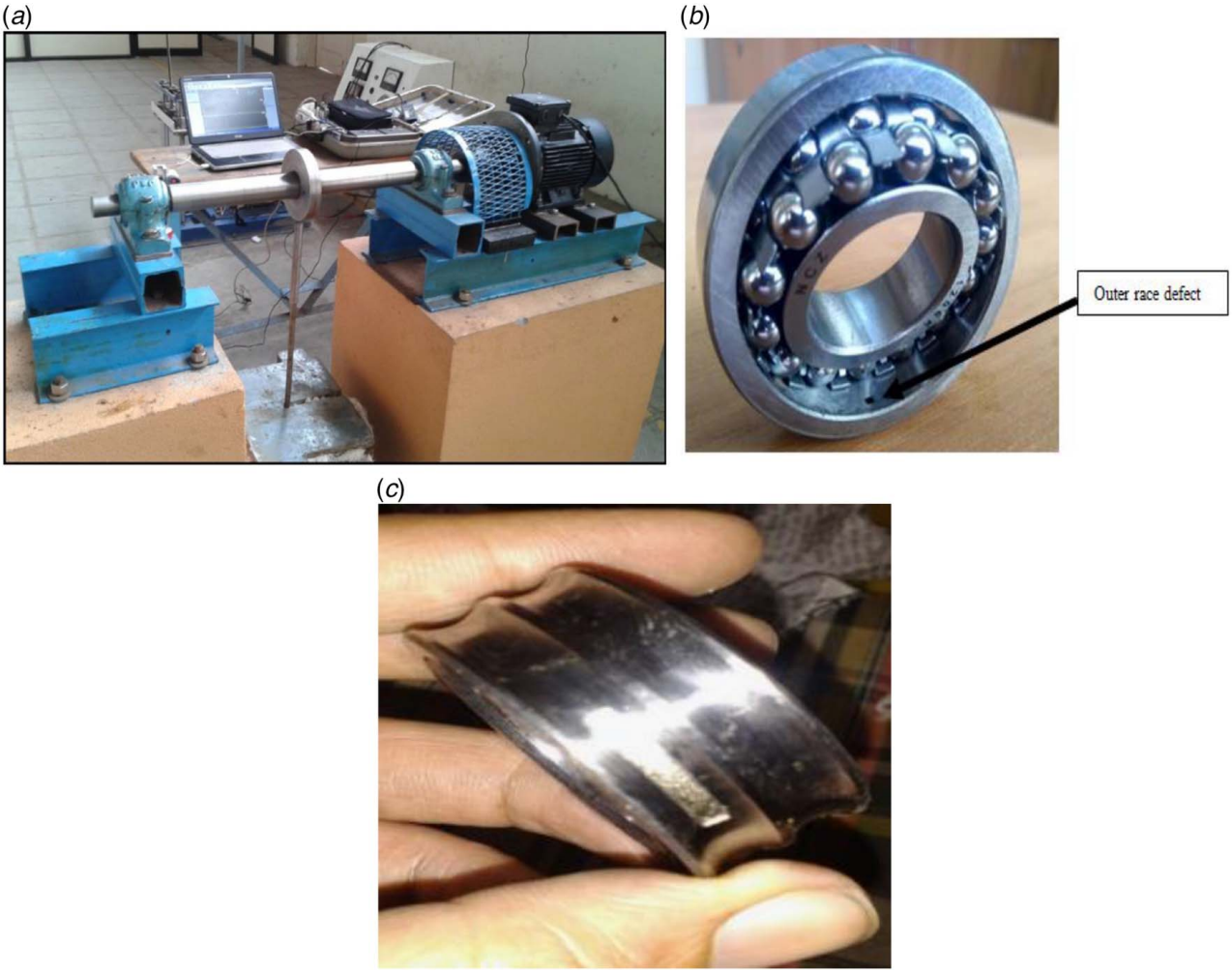

Fig. 5 (*a*) Comprehensive simulation test rig for mechanical failure, (*b*) bearing outer ring failure, and (c) bearing inner race failure

subspace vectors generated by each layer of decomposition are orthogonal in the deep VMD-ICA algorithm proposed in this paper.

When using the deep VMD-ICA algorithm proposed to detect faults, the covariance of the dataset S is expressed as follows [7]:

$$S = \frac{1}{N-1}(X_c)^T(X_c) \tag{17}$$

According to Eq. (6), the first-order decomposition covariance of deep VMD-ICA can be expressed as

$$S = \frac{1}{N-1}(X_{c11} + X_{c12})^T \tag{18}$$

After λ-order decomposition, the covariance expression is as follows:

$$S = \frac{1}{N-1}\left(\sum_{k=1}^{2\lambda} X_{c\lambda k}\right)^T \left(\sum_{k=1}^{2\lambda} X_{c\lambda k}\right) \tag{19}$$

Since the subspace vectors generated by each layer of decomposition are orthogonal in the deep VMD-ICA algorithm, there are

$$(X_{c\lambda k})^T(X_{c\lambda k+1}) = 0 \tag{20}$$

The simplified formula of (19) is

$$S = \frac{1}{N-1}|(X_{c\lambda k})^T(X_{c\lambda k})| \tag{21}$$

Therefore, $S_{\lambda k} = \frac{1}{N-1}X_{c\lambda k}^T X_{c\lambda k}$, then the covariance matrix can be expressed as

$$S = \sum_{k=1}^{3} S_{2k} + S_{24} = \sum_{k=1}^{2} S_{\lambda k} + S_{\lambda 2^{\lambda}} \tag{22}$$

where, $\sum_{k=1}^{2\lambda k} S_{\lambda k} > \ldots > \sum_{k=1}^{3} S_{2k} > S_{11}$. Since the size of the covariance describes the amount of information stored in each dimension, it can be seen from the above Eq. (22) that the amount of information stored is continuously increasing when the dataset is continuously decomposed. For this reason, we infer that the use of deep VMD-ICA method can retain more fault information during fault detection, and better complete incipient fault detection.

Table 1 Configured bearing parameters analyzed

Parameters	Value
Sleeved self-aligning ball bearing	6203
Inner diameter, mm	17
Outer diameter, mm	40
Width, mm	12
Ball diameter, mm	8
Pitch diameter, mm	48
Number of balls	29
Dynamic load rating, N	9600
Max. allowable rotational speed, rpm	18,000

Table 2 Deterministic characteristic defect frequencies

Shaft rotation (N), rpm	Rotating frequency (f_s), Hz	Quantity of rollers (Z)	Compliance frequency (CF), Hz	Defective frequency, Hz			
				f_i	f_o	f_c	f_r
750	15	29	155	219	155	6	37
1150	18	29	194	275	194	6	48
1500	22	29	231	329	231	8	58

Based on Eqs. (6)–(15), it decomposes the VMD-processed data into a third-order decomposition. For the first-order decomposition, the residual subspace is X_{c12}, the second-order decomposition residual subspace is X_{c24}, and the third-order decomposition residual subspace is X_{c38}. Through the detailed geometric relationship described in Fig. 2, the remaining amount of X_{c12} is greater than X_{c24}, while the remaining amount of X_{c24} is greater than X_{c38}, then we can conclude that after the deep decomposition principle is used, more subtle fault information can be mined, which is conducive to incipient fault detection. Vibration amplitude of VMD for fault detection with time and power/frequency is shown in Fig. 3. The amplitude for healthy decomposition with higher and lower resonance waveforms is shown in Figs. 3(*a*) and 3(*b*). The lower-resonance elements are composed of non-oscillatory transients of unpredictable shape and length. The higher-resonance components are constituted of numerous simultaneous sustained oscillations. The instantaneous frequency of d_1 and d_2 is $f_{d_1}(t) = 60 + 200t$ and $f_{d_2}(t) = 130 + 500t$ as shown in Figs. 3(*c*) and 3(*d*) for unhealthy decomposition.

2.4 Control Limits and Statistics. This section presents the calculation method of the control limit and statistics of the deep VMD-ICA method for fault detection, then judges whether the fault occurs by comparing the size relationship between the two.

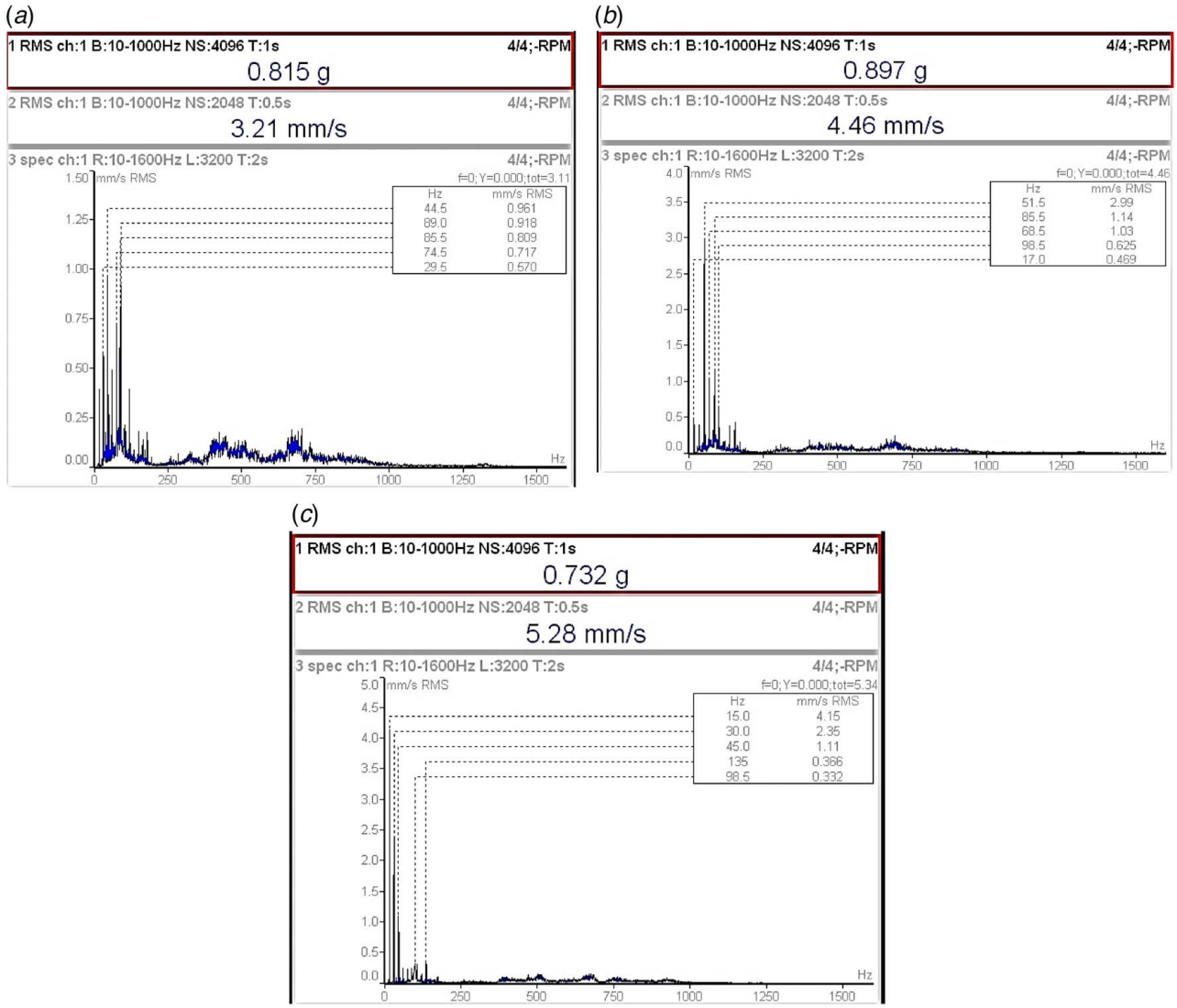

Fig. 6 Frequency spectra at (*a*) 750 rpm with fault of 5 × 0.5 × 0.1 mm, (*b*) 1150 rpm 10 × 1.5 × 0.3mm, and (*c*) 1500 rpm 15 × 2 × 0.4 mm

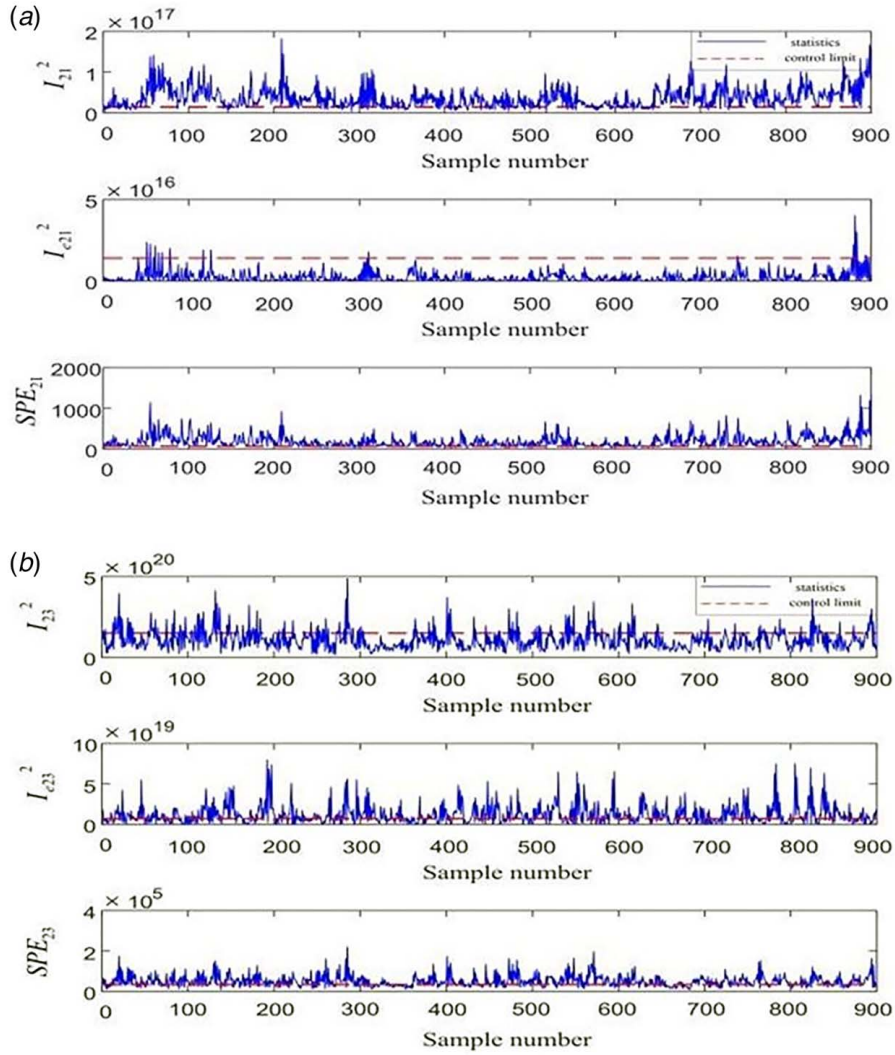

Fig. 7 (*a*) Fault indicator for 0.5 mm localized fault at 750 rpm based on ICA and (*b*) fault indicator for 1.5 mm localized fault at 1150 rpm VMD-ICA

First, calculated statistics $I_{ck\lambda^2}$, $I_{eck\lambda^2}$, $\mathrm{IPE}_{ck\lambda}$, under normal conditions, and then the kernel density estimation method to evaluate the control limits of the corresponding statistical data. For the sampled data $x_{newct}|k|$ at a certain time k, the corresponding independent components can be calculated by the separation matrices W_d and W_e [8]

$$\hat{S}_{newd}|k| = W_d x_{newct}|k| \tag{23}$$

$$\hat{S}_{newd}|k| = W_e x_{newct}|k| \tag{24}$$

I^2 is the statistics of the main model, which is the standard sum of squares of the main independent elements $\hat{S}_{newd}|k|$ at time k, and is the internal representation of the model, defined as follows:

$$I^2|k| = \hat{S}^T_{newd}|k|\hat{S}_{newd}|k| \tag{25}$$

I_e^2 is the statistic of the auxiliary model. Incorrect selection of the number of independent components, the model will compensate for the error to realize fault detection. The definition is as follows:

$$I_e^2|k| = \hat{S}^T_{newe}|k|\hat{S}_{newe}|k| \tag{26}$$

SPE is the statistic of the change of the residual model. At the sampling time k

$$\mathrm{SPE}\ |k| = e|k|^T e|k| = \{x_{newct}|k| - \hat{x}_{newct}|k|\} \tag{27}$$

where $\hat{x}_{newct}|k| = \mathrm{SPE}^{-1}B_d W_d x_{newct}|k|$.

The online detection is realized through the detection model established in Eq. (27) and the relationship between the statistics and the control limit is compared to determine whether the fault has occurred. When the calculated statistic is above the control limit, it is determined that the fault has occurred, otherwise no fault has occurred. At the same time, the calculated control limit will affect the final detection effect. When the control limit is selected too high, some fault data cannot be detected, resulting in a higher rate of false negatives; when the control line is too low, some normal data will be considered as fault data, resulting in a higher false alarm rate. Therefore, the determination of the control limit is an important link and is completed in the offline phase. The value of the statistics in the online phase is calculated from the online data.

2.5 Process of Deep VMD-ICA Algorithm Detection. The development of an intelligence rolling bearing fault diagnosis system is the main objective of this research. However, the variable operating conditions of roller bearings cause some complexities and instability in vibration signal collection. The model's poor extrapolation performance based on the traditional method would fail to

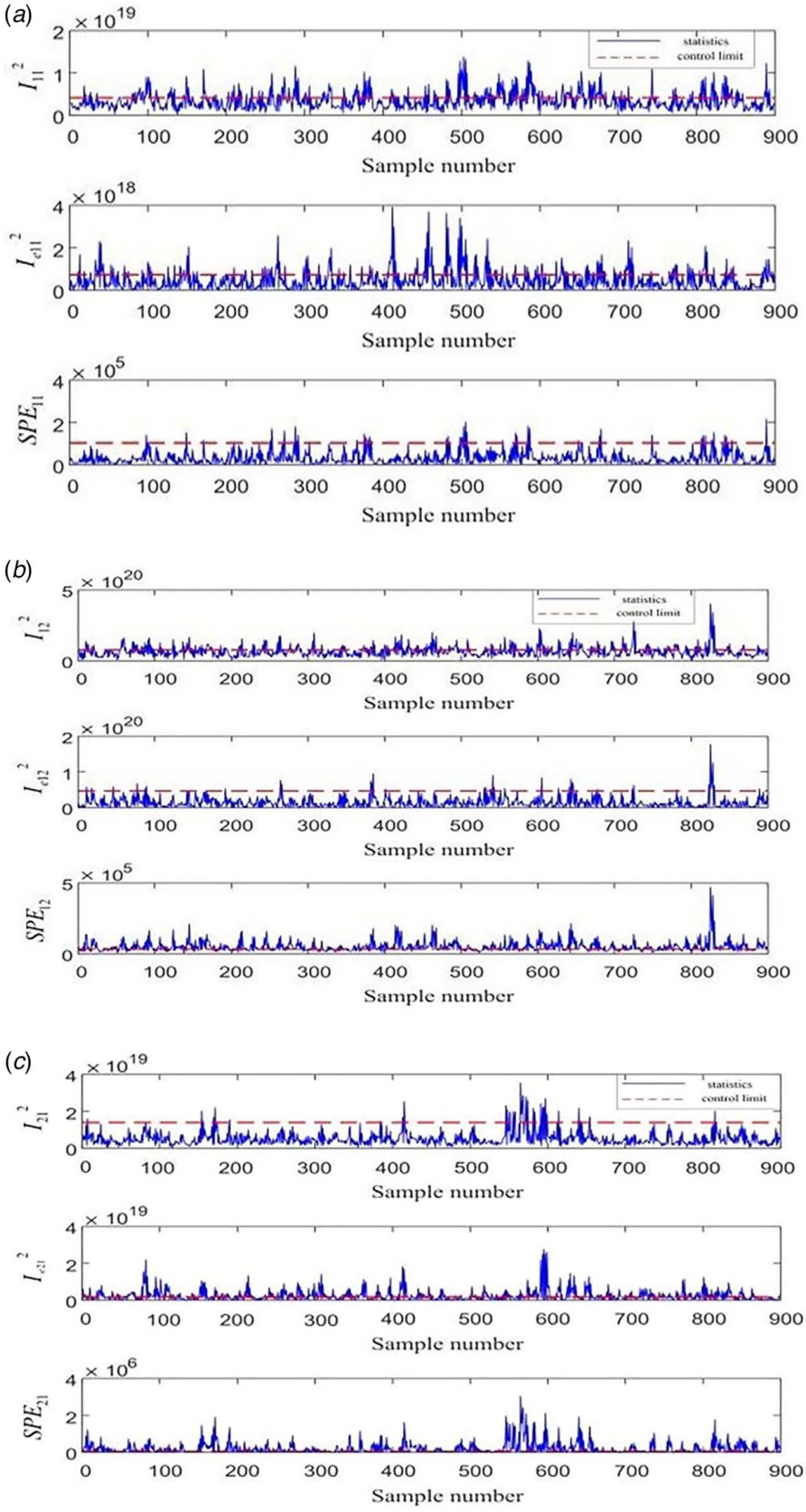

Fig. 8 Outer race experimental results based on deep VMD-ICA

diagnose bearing faults under such variable conditions. Traditional VMD has decomposability and certain endpoint effect phenomena in nature. To reduce its effects, original data are decomposed under first, second, third order up to nth order based on deep VMD-ICA under the principle of deep decomposition theory. To improve the performance of the DICA method, this is based on the VMD fault diagnosis model, in a complex and changing environment. The DICA-VMD algorithm is used to perform simultaneous signal

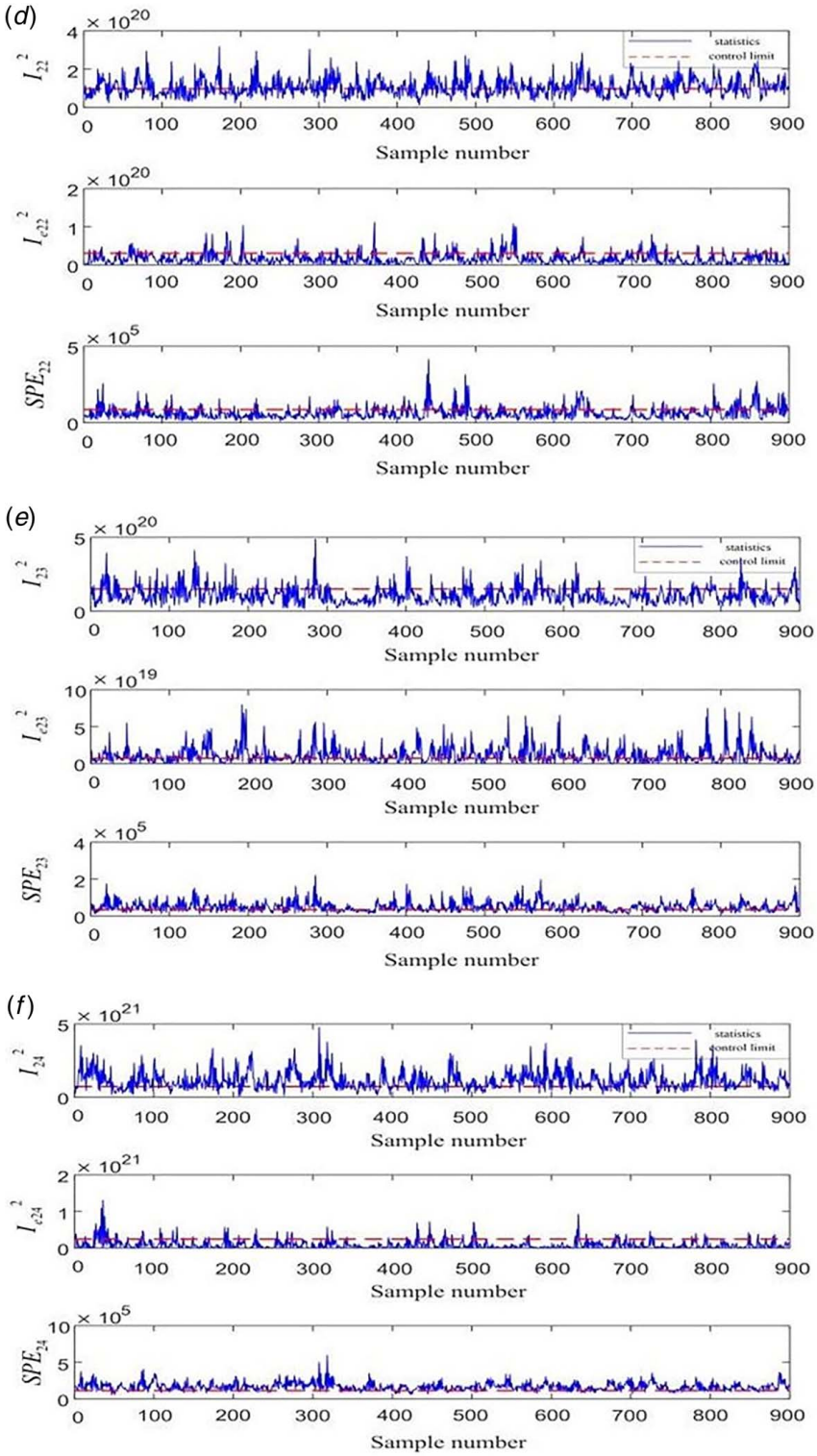

Fig. 8 ***Continued***

filtering and data enhancement. A non-stationary compound signal can be automatically divided into several IMF components by VMD to provide time-frequency contents [42]. The process flow diagram for the deep DICA-VMD algorithm detection is shown in Fig. 4.

3 Experiments With Real-World Data

As shown in Fig. 5(*a*), an experimental test rig was employed to produce the vibration signals used in this work. This test rig includes a variety of attachments for introducing faults. The significant parts of the test rig are a three-phase induction motor of 2 HP, a modular coupler, a flexible coupling, two pedestal blocks, two deep groove ball bearings, a motor controller variable frequency drive (VFD), and a radial load. A vibration isolation mounting is provided for supporting the system. The base support of the induction motor is the closest, and the second support is another end at a distance of 1.3 m. Various predefined faulted bearings from 0.5 mm to 2.5 mm faults in the outer and inner race, balls in a fault

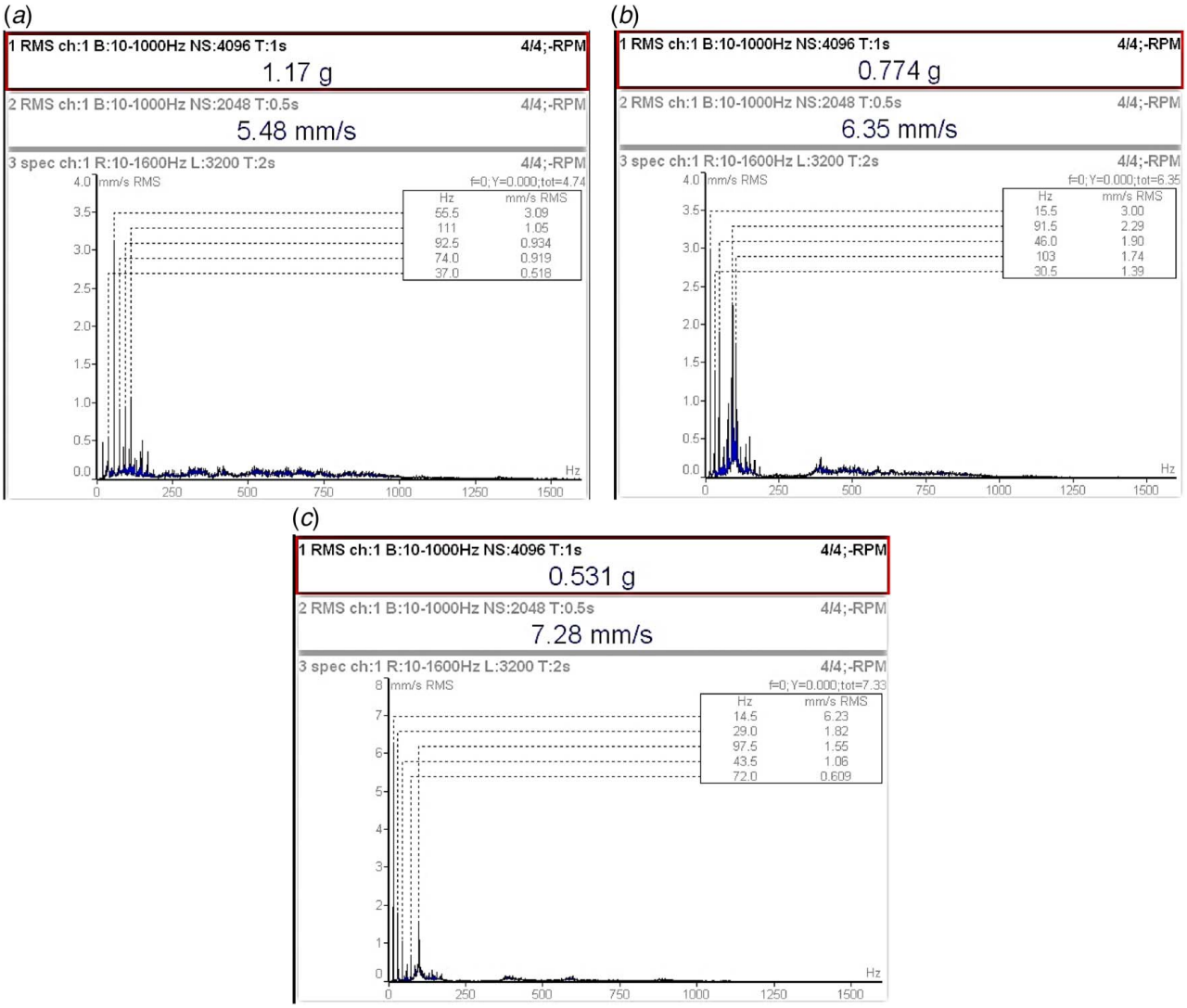

Fig. 9 Frequency spectra for inner race defect: (*a*) 750 rpm with fault of 5 × 0.5 × 0.1 mm, (*b*) 1150 rpm with fault of 10 × 1.5 × 0.3 mm, and (c) 1500 rpm with fault of 15 × 2 × 0.4 mm

sequence, are used for experiments. A circumferential loader is placed in the center of two bearing blocks to impose radial load on the testing bearings. A VFD is employed to control the rotor shaft speed from 750 rpm to 1500 rpm. A varying load of 150–500 N is applied radially for loading arrangement. To measure vertical and horizontal vibrations, a piezoelectric accelerometer with a sensitivity of 110 mV/g is attached to the far-bearing housing [25]. The Adash 1000 (fast Fourier transform) analyzer collects and processes vibration signatures. Table 1 lists relevant data on the bearing parameters. The vibrational velocity of the pedestal is also measured using a polytec laser vibrometer [37].

First, tests with both healthy and unhealthy self-aligning deep groove ball bearings are conducted. At 750 rpm, 1150 rpm, and 1500 rpm, a sum of 55 vibration signers is collected. The vibration signals are recorded at a sample rate of 24,500 Hz for a specified revolutions per minute (RPM). For a specific RPM, the vibration signals are recorded at a sample rate of 24,500 Hz. Second, using an electric discharge machine (EDM), artificial both outer and internal race defects are formed (Figs. 5(*b*) and 5(*c*)). The faults have dimensions of 5 × 0.5 × 0.1 mm, 10 × 1.5 × 0.3 mm, and 15 × 2 × 0.4 mm. The scale of the defects that are formed simulates the size of faults that are typically seen at the beginning of the deterioration of bearings [34]. The vibration fault characteristics frequencies for 750, 1150, and 1500 rpm shaft speeds are shown in Table 2.

In contrast to distributed faults, localized defects exhibit straightforward vibration signals. Distributed faults include a number of minute vibrations as well as two dominant excitation responses at the exit and entry points. At the outer race's ball pass frequency (BPFO), a localized defect in the bearing will cause impulse reactions. Each rolling element will strike the damaged area once per cage frequency if they are of the same size and spacing apart. As a matter of fact, rolling elements collide with the defective surface during each cage rotation, generating $\mathrm{BPFO} = Z \times f_c$. Inner race defects produce additional intricate vibration signatures. As the defect revolves around the shaft rotation, the shaft frequencies attenuate the inner race characteristic frequency (BPFI). Variation in ball diameter has a noticeable impact when the defects are distributed. This situation, $\mathrm{BPFI} = Z \times FTF$, represents the connection between both the fundamental train frequency and the frequency of inner racial characteristics.

4 Results and Discussion

The vibration spectrum is gathered in three different experiments using a piezoelectric accelerometer mounted on a bearing pedestal. 24,500 Hz and 1 s are the sample frequency and time, respectively. An initial test is performed on the healthy bearing. With each inner race defect, a second experiment run is performed. Each outer race

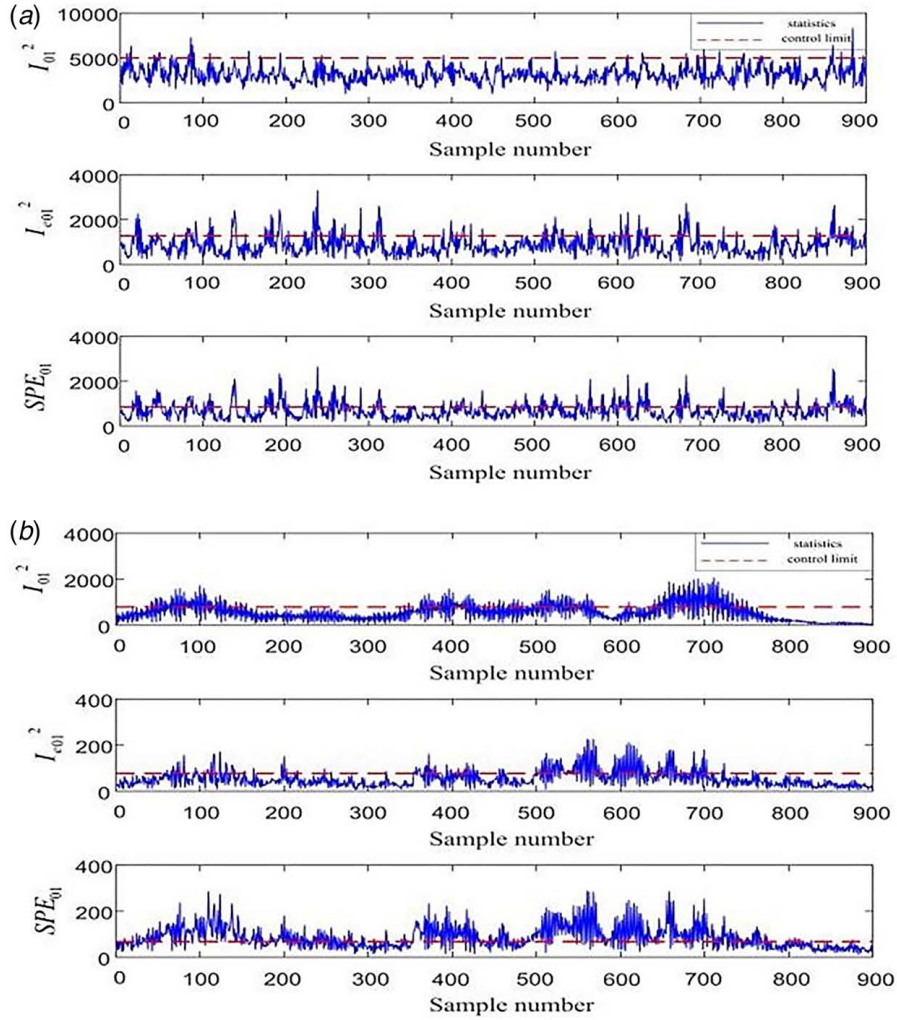

Fig. 10 (*a*) Fault indicator for 1.5 mm localized fault at 750 rpm based on ICA and (*b*) fault indicator for 2.5 mm distributed fault at 1500 rpm VMD-ICA

fault is used in a third experiment run. For each type of experiment, the shaft is rotated at varied speeds of 750, 1150, and 1500 rpm. For each case, the findings are explained below.

4.1 Unhealthy Bearing's Vibration Response. Whenever the rolling elements are positioned the cage rotates with a rotating frequency, the outer racial emits and passes parameterized excited vibrations. The characteristic frequency $Z \times f_c$ of these vibration signals is BPF, also known as changing compliance frequency. Figure 6 displays the vibration amplitude in millimeters per second of an unhealthy bearing at 750, 1150, and 1500 rpm with radial load of 150–500 N. Ring waviness results in the observation of many peaks [35].

4.2 Localized Outer Race Defect. One of the most frequent localized bearing faults is spalling or pitting. A problem with the rolling bearing outer ring surface occurs when the impact will arise when these defects pass through during the bearing rotation. The larger the defect, the greater the pulse force generated. Since the fault diameter of the bearing defect selected in this experiment is very small, and the characteristic signal generated by vibration and shock is weak, this section can well simulate the detection effect when the outer ring has a weak fault. An excitation frequency is known as the rolling element passing frequency linked to the vibration responses of the testing bearing with an outer race defect. This excitation can periodically interact with the bearing cage frequency. The experimental test rig rotor has a faulty bearing installed at the non-drive end with dimensions of 1 mm deep by 3 deg wide on the outer race. Figure 7 shows vibration spectra for localized fault at 750 rpm and 1150 rpm. Peak amplitude for these speeds seems numerous of the outer race bearing defect. Due to rotor rotation and the sidebands of the outer race ball pass frequency, some additional peaks are visible. Further monitoring charts for faults 0.5 mm and 1.5 mm are presented in Figs. 7(*a*) and 7(*b*) to further illustrate the excellence of VMD-ICA. The two indices' control limitations in terms of a 99% confidence level are represented by the horizontal lines. In Fig. 7(*a*), the majority of the points in the ICA chart I_{11}^2 are beyond the control limit, and the majority of the points in the SPE_{11} chart are also much above control limit. However, a significant percentage of the points in Fig. 7(*b*) I_{21}^2 and SPE_{23} are outside the control limit. According to the VMD-ICA algorithm's utilization of higher-order statistical data in Eq. (27), both I_{11}^2 and SPE_{11} of the ICA-related approaches provide much high rates of detection. In Fig. 7(*a*), ICA detects the faults at sample number of 620 and in Fig. 7(*b*) VMD-ICA detects the fault at 300 sample number. It can be observed that at 750 rpm peak amplitude occur at $3.5f_0$ (80 Hz) and $10f_0$ (191 Hz) with 600 sample number statistics in I_{11}^2, above control limit values of healthy bearings. SPE_{22}, I_{22}, and SPE_{11} statistics have a lesser impact on the failure of the rolling bearing localized outer race defect.

Figures 7(*a*) and 7(*b*) respectively use the traditional ICA and VMD-ICA to detect the faults. The above experimental result

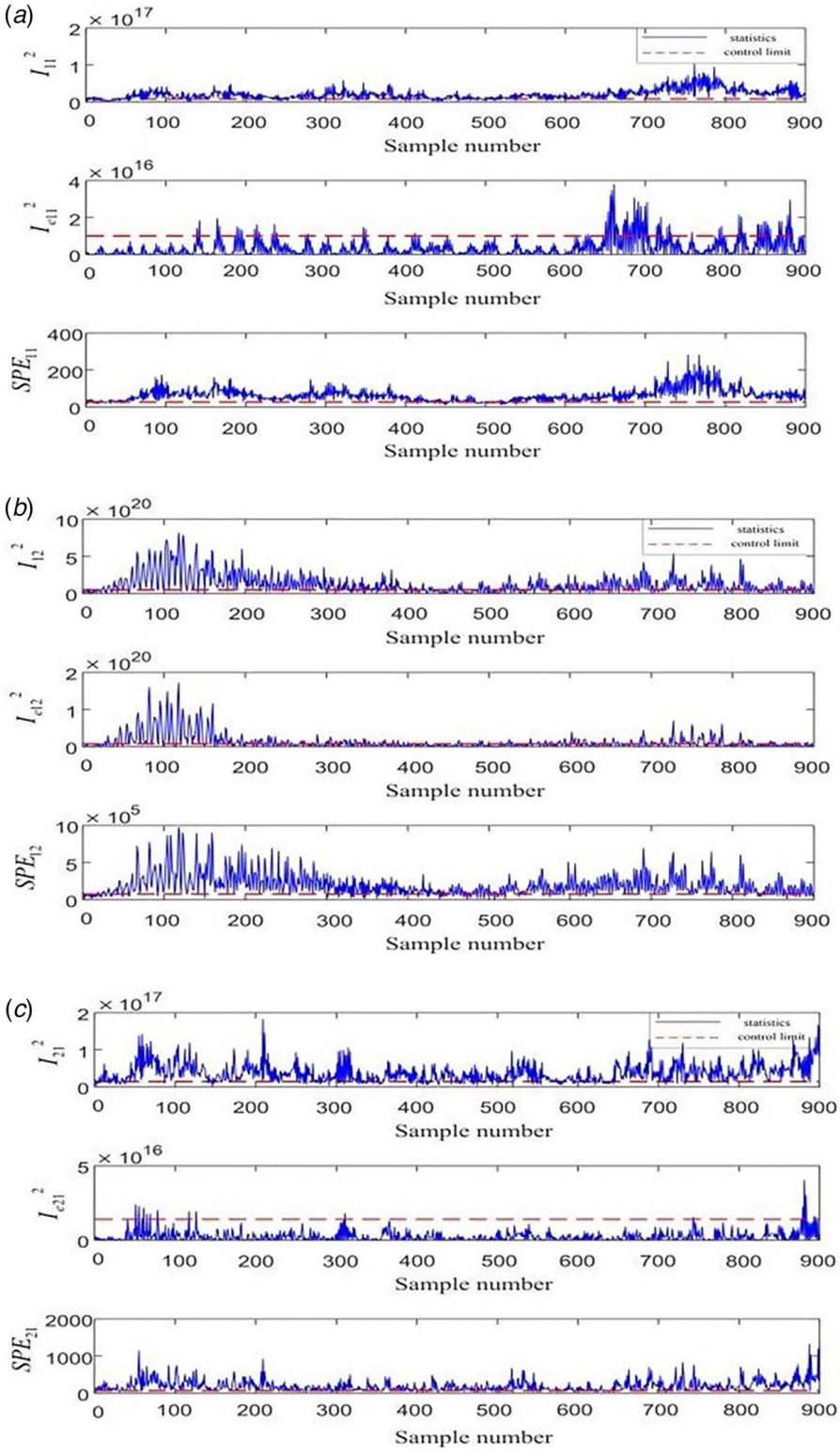

Fig. 11 Inner race experimental results based on deep VMD-ICA

indicates that the VMD-ICA method has a better effect on fault detection, but the false negative rate exceeds 40%, which is still quite high. Figures 8(*a*) and 8(*b*) describe the results of using the deep VMD-ICA method to detect the second-order of data. Compared with the detection result of the first layer, the false negative rate is reduced, and the 12 statistics are more sensitive to rolling SPE bearing failure. Figures 8(*c*)–8(*f*) describe the results of using the deep VMD-ICA method to detect the third layer of data. Compared with the detection results of the first two layers, the false negative rate and delay rate are significantly reduced. The statistics SPE_{21}, Ie_{12}, and SPE_{24} have a greater impact on the fault. Therefore, after the third-order decomposition, and detection effect is better.

4.3 Distributed Inner Race Defect. On the outer race, a distributed artificial fault is developed and is distributed over 52 deg

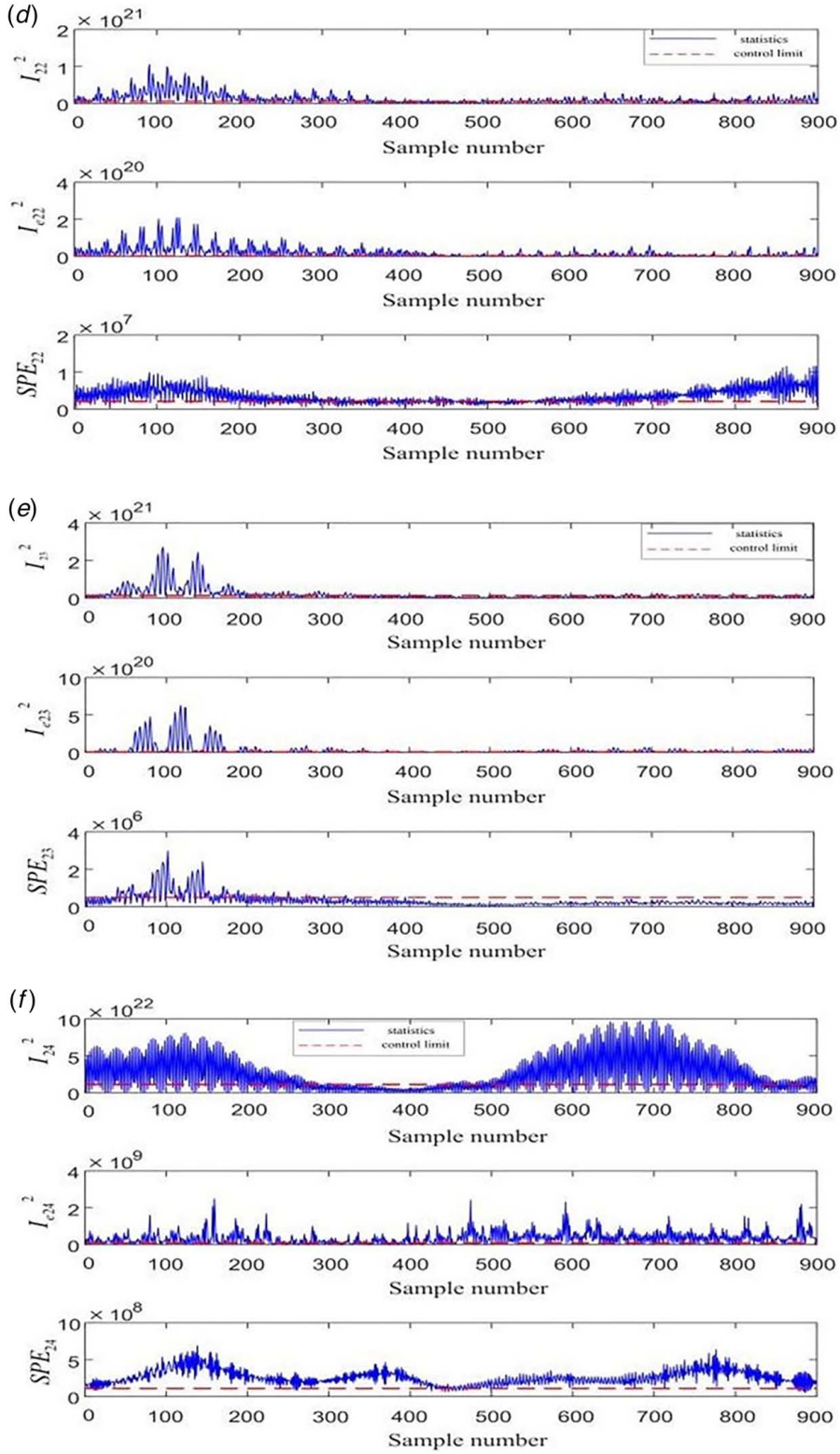

Fig. 11 ***Continued***

of the race's circumference. Figure 9 illustrates the frequency response at various speeds. The characteristic frequency of an inner race defect BPFI indicates the existence of an inner race defect. There are distributed inner race defects, as shown by the peak at FTF and harmonics. Local and spread defects can be distinguished from one other using the harmonics. The theoretic model Eq. (27), the expected vibrational amplitude closely matched the findings of the experiment. For shafts rotating at different speeds, it is clear that the theoretical and experimental vibration amplitude values agree reasonably well.

Figure 10 shows vibration spectra for localized fault at 750 rpm and 1500 rpm. Further monitoring charts for faults 1.5 mm and 2.5 mm are presented in Figs. 10(*a*) and 10(*b*) to further illustrate the excellence of VMD-ICA. The majority of the points I_{01}^2 in the

Table 3 Comparison of fault detection rate (%)

Detection methods	ICA		VMD-ICA		Deep ICA		Deep VMD-ICA		DPCA		KPCA		KDPCA		DICA		KICA	
	I^2	SPE	I^2	SPE	I^2	SPE	I^2	SPE	I^2	SPE	I^2	SPE	I^2	SPE	I^2	SPE	I^2	SPE
0.5 mm defect (Outer race)	98.5	99.1	**100**	99.3	99.5	99.2	**97.2**	**100**	85.1	86.7	45.1	45.9	98.1	98.9	12.3	12.1	98.4	98.7
1.0 mm defect (Outer race)	99.1	99.3	89.1	**100**	99.1	99.6	**99.6**	**100**	76.1	75.4	99.5	99.1	75.2	76.4	99.1	99.9	75.1	76.9
1.5 mm defect (Outer race)	95.2	98.1	93.3	94.2	95.1	96.2	**98.2**	**99.9**	**100**	**100**	62.3	62.1	98.4	98.9	**100**	99.6	**100**	99.1
2.0 mm defect (Outer race)	98.1	98.3	94.1	95.4	98.5	98.7	**97.4**	**99.4**	61.3	62.2	73.2	74.2	97.1	98.9	77.1	76.5	89.5	88.1
2.5 mm defect (Outer race)	**100**	99.4	88.2	90.2	99.1	**100**	**99.5**	**100**	100	99.6	42.3	44.5	**100**	**100**	14.9	15.2	46.1	45.6
0.5 mm defect (Inner race)	98.1	97.2	85.6	87.3	98.2	**100**	**96.9**	**98.9**	54.9	53.2	**100**	**100**	96.4	97.9	88.2	88.9	58.4	59.4
1.0 mm defect (Inner race)	94.3	91.5	95.2	**100**	94.0	95.1	**98.5**	**100**	78.3	79.1	92.7	91.8	17.5	18.3	99.5	99.1	13.1	12.7
1.5 mm defect (Inner race)	91.2	88.6	91.1	91.9	95.8	96.7	**99.1**	**99.2**	95.6	99.5	85.5	87.4	45.9	46.1	88.4	89.6	35.1	36.8
2.0 mm defect (Inner race)	87.1	87.3	88.2	88.6	95.1	93.1	**99.6**	**100**	99.5	96.2	93.8	93.4	55.1	55.1	**100**	**100**	56.1	55.4
2.5 mm defect (Inner race)	92.9	93.7	**100**	92.9	**100**	99.2	**99.8**	**99.8**	95.7	96.8	**100**	**100**	92.3	93.4	95.7	96.1	**100**	**100**

Note: The bold typeface indicates the greatest detection rate.

ICA chart in Fig. 10(*a*) are lower than the control limit. Similarly to this, the majority of the points on the SPE_{01} chart are within the control limit. However, the majority of the points in Fig. 10(*b*) SPE_{01} are above the control limit and I_{01}^2 is in between control limit. In Fig. 10(*a*), ICA detects the faults at sample number of 600 and in Fig. 10(*b*) VMD-ICA detects the fault at 620 sample number.

Figures 11(*a*) and 11(*b*) show the detection results of fault data when using the deep VMD-ICA method for second-order decomposition, SPE_{11}, I_{11}, and SPE_{12} statistics have a greater impact on the failure of the rolling bearing inner race. Figures 11(*c*)–11(*f*) describe the detection results of deep VMD-ICA three-order decomposition, the statistics SPE_{21}, Ie_{22}^2, and SPE_{24}, have a greater impact on outer circle faults, which shows that the deep VMD-ICA third-order decomposition has a better fault detection effect. It can be observed that at 1500 rpm peak amplitude occur at $5.5f_0$ (120 Hz) and $15f_0$ (201 Hz) with 100 sample number statistics in I_{12}^2, above control limit values of healthy bearings. SPE_{12}, I_{12}, and SPE_{12}, SPE_{22}, statistics have a higher impact on the failure of the rolling bearing distributed inner race defect.

4.4 Comparison of Experimental Results. The comparison of I^2 and SPE for different detection techniques are measured for various defects at various speeds is shown in Table 3. It can be seen that when speed rises, the vibration's amplitude for the outer race local increases. For the same load, a distributed outer race fault results in a lower vibration amplitude at all RPMs than a local outer race fault. The vibration amplitude is higher on the side at all RPMs when the outer race fault is local, and the inner race fault is distributed for the same load. Irrespective of the defect type, the vibration's amplitude grows as the RPM rises. Additionally, it verified that vibration amplitude invariably increases with increasing load regardless of the defect type. As a result, the main variables in rotor-bearing systems are load and speed. The majority of the error falls within allowable limits and closely matches with the theoretical model predicted by Eq. (27) for both the vibration amplitude and the defective frequency.

Table 3 compares the performance of the above nine rolling bearing fault detection methods. The bold typeface indicates the greatest detection rate numbers for certain defects. The results indicate that deep VMD-ICA provides the highest detection rates for almost all defects. For fault sizes of 2 mm and 2.5 mm, the fault detection rates are nearly 100% due to the higher magnitude generated due to faults. Similarly, for smaller fault size there is no effect in other compared techniques. Moreover, every method has dual indices for results one for fair and the other for average detection rate. It is estimated that deep VMD-ICA outperforms compared to traditional techniques, respectively. Since deep VMD-ICA uses the advantage of high-order statistics to identify and extract independent components. However, PCA merely extracts unrelated components using mean value and variance. Deep VMD-ICA, on the other hand, is more effective than any other method since it considers dynamics, non-linearity, and non-Gaussianity all at once. The experimental results show that the traditional ICA and VMD-ICA method has a low fault detection rate and a detection delay, so the effect of using them for incipient fault detection is not good. On the contrary, the deep ICA and deep VMD-ICA methods have a higher fault detection rate and most of the faults can be detected and there is almost no detection delay. At the same time, the deep VMD-ICA method shows better performance due to the processing of noise.

4.5 Validation of Model. Fifty-three more experiments are conducted on the races of DGBB with varying fault sizes to confirm the validity and performance of the model. EDM is used to produce faults with sizes of $5 \times 0.5 \times 0.1$ mm, $10 \times 1.5 \times 0.3$ mm, and $15 \times 2 \times 0.4$ mm. The proposed model, shown in Eq. (27) is utilized to compute the vibration characteristic frequencies and amplitudes. As shown in Table 4, the estimated amplitudes

Table 4 Testing the validity of vibration amplitudes experiments

Defect position	Speed, rpm	Load, N	Experimental trial amplitude, mm/s	Models amplitude, mm/s	Absolute error	Experimental trial frequency, Hz	Models frequency, Hz	Absolute error
Local outer race	750	150	0.56	0.54	5.81	199	196.12	3.91
	1150	150	2.64	2.96	4.32	212	231.25	5.24
	1500	150	2.13	2.48	2.08	245	284.36	0.136
Distributed outer race	750	150	0.523	0.691	11.12	190.23	198.25	3.684
		300	0.912	1.56	13.71	205.21	214.31	1.687
		500	1.125	1.78	1.33	205.65	214.36	4.325
	1150	150	0.758	1.16	7.56	198.21	207.25	7.12
		300	1.274	1.86	8.14	206.23	208.12	1.624
		500	2.875	2.91	2.31	204.23	195.45	2.693
	1500	150	0.452	0.62	15.32	188.49	198.25	2.145
		300	1.351	1.83	2.12	207.84	195.45	4.256
		500	2.896	3.16	3.45	201.36	188.91	3.248
Distributed inner race	750	150	0.635	0.754	15.21	194.52	219.73	2.145
		300	0.524	0.637	12.45	212.82	198.52	3.657
		500	0.983	0.945	3.25	192.45	184.32	0.133
	1150	150	0.124	0.168	8.45	185.25	205.12	12.364
		300	0.986	0.914	2.36	212.69	215.63	10.256
		500	1.478	1.461	5.34	183.24	200.81	6.52
	1500	150	2.231	2.345	7.69	185.64	206.34	4.971
		300	1.038	1.045	8.28	203.87	209.78	5.261
		500	1.725	1.751	8.36	198.56	199.45	7.069

are analyzed with the experimentally measured amplitudes. Table 4 compares experimental and model values for the local outer race, outer race fault, and distributed inner race faults for various shaft rotational speeds between 750 rpm and 1500 rpm, as well as the associated errors of the three cases.

A novel approach for incipient fault detection of a distributed bearing defect is suggested based on the findings of the experimental analysis and the results of the theoretical model. By comparing the amplitudes of two characteristic frequencies for the outer and inner races, respectively, BPFO; FTF and BPFI; FTF, it is possible to identify the distributed fault. Additionally, it has been found that localized faults only excite at BPFO or BPFI. There is a significant percentage of agreement between experimental and theoretical values. With a relative error of less than 11%, the suggested model accurately predicts the behavior of distributed defects on roller bearings.

5 Conclusion

The rolling bearing data gathered in engineering practice are non-Gaussian data. The rolling bearing has weak incipient fault characteristics and is disordered with noise, a novel method called deep VMD-ICA is proposed in this research work to detect the incipient fault.

Considering noise processing, the proposed deep VMD-ICA has a better incipient fault detection effect than the ICA method. The deep VMD-ICA introduces the principle of deep decomposition, and can fully dig out incipient failure characteristics information, which is conducive to detecting the incipient fault.

Deep VMD-ICA integrates ICA, VMD, and deep decomposition. It also retrieves the characteristic features of auto-correlation, cross-correlation, and non-linearity. The defect diagnostics are accomplished by using a non-linear contribution plot that is built on partial derivatives and linear contributions. Additionally, the Tennessee Eastman technique was used to compare deep VMD-ICA to linear dimensionality reduction technique (DPCA), kernal principal component analysis (KPCA), kernal dynamic principal component analysis (KDPCA), discrete imperialist competitive algorithm (DICA), and kernal independant component analysis (KICA). The experimental findings show that deep VMD-ICA has the best fault detection performance, utilizes more information than standard approaches, and contributes accurate incipient fault detection. Through the experimental results analysis, we can get the fault detection rate of the deep VMD-ICA method reaches about 98% and there is almost no detection delay, some incipient weak fault characteristics can be better detected. Evaluating the level of the non-Gaussian non-linear process is still a challenge. 11% of the experimental values deviate from the theoretical model, with $R^2 = 0.98$. To conclude, further studies are needed to strengthen the proposed method.

The prognosis and estimated tarrying life of the bearings can be determined using the suggested bearing diagnosis procedure. Additionally, this work can be expanded to include additional soft computing techniques for rotating systems fault identification and experimental investigation.

Conflict of Interest

There are no conflicts of interest.

Data Availability Statement

No data, models, or code were generated or used for this paper.

References

[1] Stefatos, G., and Hamza, A., 2010, "Dynamic Independent Component Analysis Approach for Fault Detection and Diagnosis," Expert Syst. Appl., **37**(1), pp. 8606–8617.

[2] Fan, J., and Wang, Y., 2013, "Fault Detection and Diagnosis of Non-Linear Non-Gaussian Dynamic Processes Using Kernel Dynamic Independent Component Analysis," J. Inf. Sci., **47**(18), pp. 6961–6971.

[3] Mao, W., Ding, L., Tian, S. T., and Liang, X., 2020, "Online Detection for Bearing Incipient Fault Based on Deep Transfer Learning," Measurement, **152**(1), p. 107278.

[4] Cai, L., Tian, X., and Chen, S., 2014, "A Process Monitoring Method Based on Noisy Independent Component Analysis," Neurocomputing, **127**(1), pp. 231–246.

[5] Cai, L., and Tian, X., 2014, "A New Fault Detection Method for Non-Gaussian Process Based on Robust Independent Component Analysis," Process Saf. Environ. Prot., **92**(6), pp. 645–658.

[6] Cai, L., Zhu, L., and Ni, C., 2018, "Chatter Detection in Milling Process Based on VMD and Energy Entropy," Mech. Syst. Signal Process., **105**(1), pp. 169–182.

[7] Wang, Z., Chen, J., Dong, G., and Zhou, Y., 2011, "Constrained Independent Component Analysis and Its Application to Machine Fault Diagnosis," Mech. Syst. Signal Process., **25**(7), pp. 2501–2512.

[8] Yu, G., Jing, N., Bin, L., and Rong-Fong, F., 2014, "Envelope Extraction Based Dimension Reduction for Independent Component Analysis in Fault Diagnosis of Rolling Element Bearing," J. Sound Vib., **333**(13), pp. 2983–2994.
[9] Iseli, E., Guenat, E., Tresch, R., and Schiffmann, J., 2019, "Analysis of Spiral-Grooved Gas Journal Bearings by the Narrow Groove Theory and the Finite Element Method at Large Eccentricities," ASME J. Tribol., **142**(4), p. 041802.
[10] Benwei, L., and Yun, Z., 2011, "Supervised Locally Linear Embedding Projection for Machinery Fault Diagnosis," Mech. Syst. Signal Process, **25**(8), pp. 3125–3134.
[11] McFadden, P. D., and Smith, J. D., 1984, "Model for Vibration Produced by a Single Point Defect in a Rolling Element Bearing," J. Sound Vib., **96**(1), pp. 69–82.
[12] McFadden, P. D., and Smith, J. D., 1985, "Vibration Produced by Multiple Point Defects in a Rolling Element Bearing," J. Sound Vib., **98**(2), pp. 263–273.
[13] Patil, M. S., Mathew, J., Rajendrakumar, P. K., and Desai, S., 2010, "A Theoretical Model to Predict the Effect of Localized Defect on Vibrations Associated With Ball Bearing," Int. J. Mech. Sci., **52**(9), pp. 1193–1201.
[14] Dick, P., Carl, H., Nader, S., Alireza, M. A., and Sarabjeet, S., 2015, "Analysis of Bearing Stiffness Variations Contact Forces and Vibrations in Radially Loaded Double Row Rolling Element Bearing With Raceway Defect," J. Mech. Syst. Signal Process., **50–51**(1), pp. 139–160.
[15] Igarashi, T., and Kato, J., 1985, "Studies on the Vibration and Sound of Defective Rolling Bearings. Third Report: Vibration of Ball Bearing With Multiple Defects," Bull. JSME, **28**(237), pp. 492–499.
[16] Sopanen, J., and Mikkola, A., 2003, "Dynamic Model of a Deep- Groove Ball Bearings Including Localized and Distributed Defects. Part 1: Theory," Proc. Inst. Mech. Eng. K: J. Multi-body Dyn., **217**(3), pp. 201–211.
[17] Sopanen, J., and Mikkola, A., 2003, "Dynamic Model of a Deep- Groove Ball Bearings Including Localized and Distributed Defects. Part 2: Implementation and Results," Proc. Inst. Mech. Eng. J: J. Eng. Tribol., **217**(3), pp. 213–223.
[18] Tandon, N., and Choudhury, A., 1997, "An Analytical Model for the Prediction of the Vibration Response of Rolling Element Bearings Due to Localized Defect," J. Sound Vib., **205**(3), pp. 275–292.
[19] Tandon, N., and Choudhury, A., 1998, "A Theoretical Model to Predict Vibration Response of Rolling Bearings to Distributed Defects Under Radial Load," ASME J. Vib. Acoust., **120**(3), pp. 214–220.
[20] Choudhury, A., and Tandon, N., 2006, "Vibration Response of Rolling Element Bearing in a Rotor Bearing System to a Local Defect Under Radial Load," ASME J. Tribol., **128**(2), pp. 252–261.
[21] Tomovic, R., Miltenovic, V., Banic, M., and Miltenovic, A., 2010, "Vibration Response of Rigid Rotor in Unloaded Rolling Element Bearing," Int. J. Mech. Sci., **52**(9), pp. 1176–1185.
[22] Desavale, R. G., Venkatachalam, R., and Chavan, S. P., 2013, "Antifriction Bearings Damage Analysis Using Experimental Data Based Models," ASME J. Tribol., **135**(4), p. 041105.
[23] Desavale, R. G., Venkatachalam, R., and Chavan, S. P., 2014, "Experimental and Numerical Studies on Spherical Roller Bearings Using Multivariable Regression Analysis," ASME J. Vib. Acoust., **136**(2), p. 021022.
[24] Desavale, R. G., Kanai, R. A., Chavan, S. P., Venkatachalam, R., and Jadhav, P. M., 2015, "Vibration Characteristics Diagnosis of Roller Bearing Using the New Empirical Model," ASME J. Tribol., **138**(1), p. 011103.
[25] Desavale, R. G., 2019, "Dynamics Characteristic and Diagnosis of a Rotor-Bearing's System Through a Dimensional Analysis Approach: An Experimental Study," ASME J. Comput. Nonlinear Dyn., **14**(1), p. 014501.
[26] Mufazzal, S., Muzzakir, S. M., and Khanam, S., 2021, "Theoretical and Experimental Analyses of Vibration Impulses and Their Influence on Accurate Diagnosis of Ball Bearing With Localized Outer Race Defect," J. Sound Vib., **513**(1), p. 116407.
[27] Patil, S. M., Desavale, R. G., Shinde, P. V., and Patil, V. R., 2021, "Comparative Study of Response of Vibrations for Circular and Square Defects on Components of Cylindrical Roller Bearing Under Different Conditions," *Innovative Design, Analysis and Development Practices in Aerospace and Automotive Engineering*, N. Gascoin and E. Balasubramanian, eds., Lecture Notes in Mechanical Engineering, Springer, New York, pp. 189–198.
[28] Kanai, R. A., Desavale, R. G., and Chavan, S. P., 2016, "Experimental–Based Fault Diagnosis of Rolling Bearings Using Artificial Neural Network," ASME J. Tribol., **138**(3), p. 031103.
[29] Patel, V., Tandon, N., and Pandey, R. K., 2010, "A Dynamic Model for Vibration Studies of Deep Groove Ball Bearings Considering Single and Multiple Defects in Races," ASME J. Tribol., **132**(4), p. 041101.
[30] Liu, J., 2020, "A Dynamic Modelling Method of a Rotor-Roller Bearing-Housing System With a Localized Fault Including the Additional Excitation Zone," J. Sound Vib., **469**(1), p. 115144.
[31] Niu, L., Cao, H., Hou, H., Wu, B., Lan, Y., and Xiong, X., 2020, "Experimental Observations and Dynamic Modeling of Vibration Characteristics of a Cylindrical Roller Bearing With Roller Defects," J. Mech. Syst. Signal Process., **138**(1), pp. 1–19.
[32] Rafsanjani, A., Abbasion, S., Farshidianfar, A., and Moeenfard, H., 2009, "Nonlinear Dynamic Modeling of Surface Defects in Rolling Element Bearing Systems," J. Sound Vib., **319**(1), pp. 1150–1174.
[33] Yang, R., Hou, L., Jin, Y., Chen, Y., and Zhang, Z., 2018, "The Varying Compliance Resonance in a Ball Bearing Rotor System Affected by Different Ball Numbers and Rotor Eccentricities," ASME J. Tribol., **140**(3), p. 051101.
[34] Jadhav, P. M., Kumbhar, S. G., Desavale, R. G., and Patil, S. B., 2020, "Distributed Fault Diagnosis of Rotor-Bearing System Using Dimensional Analysis and Experimental Methods," Measurement, **166**(1), pp. 108239–108259.
[35] Kumbhar, S. G., Sudhagar, E. P., and Desavale, R. G., 2020, "Theoretical and Experimental Studies to Predict Vibration Responses of Defects in Spherical Roller Bearings Using Dimension Theory," Measurement, **161**(1), pp. 107846–107811.
[36] Kumbhar, S. G., and Sudhagar, E. P., 2020, "Fault Diagnostics of Roller Bearings Using Dimension Theory," ASME J. Nondestruct. Eval. Diagn. Progn. Eng. Syst., **4**(1), pp. 011001–011010.
[37] Salunkhe, V. G., Desavale, R. G., and Jagadeesha, T., 2021, "Experimental Frequency-Domain Vibration Based Fault Diagnosis of Roller Element Bearings Using Support Vector Machine," ASCE-ASME J. Risk Uncertain. Eng. Syst. B: Mech. Eng., **7**(2), p. 021001.
[38] Londhe, N. D., Arakere, N. K., and Ghatu, S., 2019, "Effect of Plasticity on the Dynamic Capacity of Modern Bearing Steels," ASME J. Tribol. Int., **133**(1), pp. 160–171.
[39] Liu, J., and Xu, Z., 2022, "A Simulation Investigation of Lubricating Characteristics for a Cylindrical Roller Bearing of a High-Power Gearbox," ASME J. Tribol. Int., **167**(1), p. 107373.
[40] Liu, J., Wang, L., and Shi, Z., 2022, "Dynamic Modelling of the Defect Extension and Appearance in a Cylindrical Roller Bearing," Mech. Syst. Signal Process, **173**(1), p. 109040.
[41] Liu, J., Xu, Z., Zhou, L., Yu, W., and Shao, Y., 2019, "A Statistical Feature Investigation of the Spalling Propagation Assessment for a Ball Bearing," Mech. Mach. Theory, **131**(1), pp. 336–350.
[42] Yan, X., Liu, Y., Zhang, W., Jia, M., and Wang, X., 2022, "Research on a Novel Improved Adaptive Variational Mode Decomposition Method in Rotor Fault Diagnosis," Appl. Sci., **10**(5), pp. 1696–1610.
[43] Fu, L., Ma, Z., Wu, D., Liu, J., Xu, F., Zhong, Q., and Zhu, T., 2022, "Bearing Cog: A Bearing Fault Diagnosis Method Under Variable Operational Conditions," Appl. Sci., **12**(10), pp. 5240–5215.